Journal of Sol-Gel Science and Technology
https://doi.org/10.1007/s10971-021-05691-y

ORIGINAL PAPER: NANO-STRUCTURED MATERIALS (PARTICLES, FIBERS, COLLOIDS, COMPOSITES, ETC.)

Photocatalytic degradation of methylene blue by flowerlike rutile-phase TiO_2 film grown via hydrothermal method

N. K. A. Hamed[1] · **M. K. Ahmad**[1] · **N. H. H. Hairom**[2] · **A. B. Faridah**[3] · **M. H. Mamat**[4] · **A. Mohamed**[5] · **A. B. Suriani**[5] · **C. F. Soon**[1] · **F. I. M. Fazli**[1] · **S. M. Mokhtar**[1,6] · **M. Shimomura**[6]

Received: 23 March 2021 / Accepted: 14 November 2021
© The Author(s), under exclusive licence to Springer Science+Business Media, LLC, part of Springer Nature 2021

Abstract

This paper presents the effects of operating parameters on the photocatalytic degradation of methylene blue using flowerlike rutile-phase TiO_2 films synthesised by a hydrothermal method. The findings show that numerous parameters such as the catalyst morphology, the presence of oxygen vacancy/Ti^{3+} surface defects, initial pH of methylene blue solution, active species, and initial concentration of methylene blue influence the photocatalytic degradation of the dye. Based on the results obtained, the presence of oxygen vacancy/Ti^{3+} surface defects act as an electron trap that helps generate more electrons and holes, which contributes to the enhancement of the photocatalytic activity of the TiO_2 film. This study reveals that the optimum concentration of Ti precursor was obtained at 0.10 M, which produced a flowerlike morphology with pristine rutile-phase that reached 42% methylene blue dye degradation. The effectiveness of the optimised film was boosted by 18% degradation by adjusting the initial pH of the methylene blue solution to 12. Under such conditions, the enhancement of the electrostatic attraction between the negatively charged TiO_2 and the methylene blue molecules improved the degradation. No severe deactivation of the catalyst was found even after five photocatalysis reaction cycles. This study also demonstrates that there are multiple parameters involved in optimising the photocatalytic activity of TiO_2.

Supplementary information The online version contains supplementary material available at https://doi.org/10.1007/s10971-021-05691-y.

✉ M. K. Ahmad
akhairul@uthm.edu.my

[1] Microelectronic and Nanotechnology–Shamsuddin Research Centre (MiNT-SRC), Faculty of Electrical and Electronic Engineering, Universiti Tun Hussein Onn Malaysia, Parit Raja, 86400 Batu Pahat, Johor, Malaysia

[2] Faculty of Engineering Technology, Universiti Tun Hussein Onn Malaysia, Parit Raja, 86400 Batu Pahat, Johor, Malaysia

[3] Faculty of Applied Sciences and Technology, Pagoh Campus, Universiti Tun Hussein Onn Malaysia, 84600 Muar, Johor, Malaysia

[4] Nano-Electronic Centre, Faculty of Electrical Engineering, Universiti Teknologi Mara, 40450 Shah Alam, Selangor, Malaysia

[5] Nanotechnology Research Centre, Department of Physics, Faculty of Science and Mathematics, Universiti Pendidikan Sultan Idris, 35900 Tanjung Malim, Perak, Malaysia

[6] Department of Engineering, Graduate School of Integrated Science and Technology, Shizuoka University, 432-8011 Hamamatsu, Shizuoka, Japan

Published online: 04 January 2022

Graphical Abstract

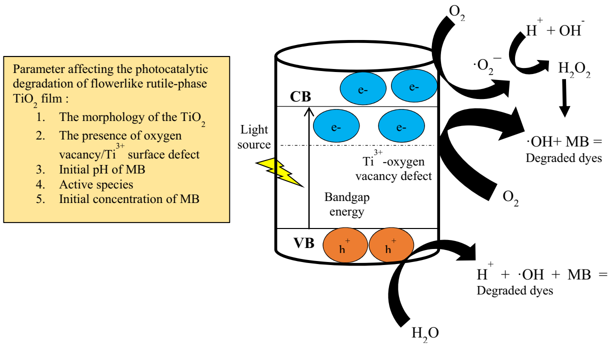

Keywords Rutile TiO_2 · Hydrothermal · Flowerlike · Photocatalysis

1 Introduction

Serious environmental and energy emissions issues are becoming some of the most challenging problems in the world. Some industries use synthetic dyes that are untreated and combined with water supplies, such as textiles, plastics, printing, etc. Synthetic dyes can cause health problems for humans and the environment [1]. One of the industrial dyes that is a cationic dye is methylene blue (MB). It is one of the most common dyeing materials for wood, silk, and cotton. A variety of illnesses, such as complications with the digestive and respiratory tracts, as well as nausea, vomiting, and profuse sweating, can be caused by excessive amounts of MB in our water resources [2]. There are diverse approaches of treatment used to remove the dye from wastewater.

A variety of treatment processes are commonly used to treat different contaminants, such as chemical oxidation, biological processes, coagulation, membrane filtration, and advanced oxidation processes (AOPs) [3–5]. For instance, AOPs have an immense capacity to handle various types of pollution and can minimise the production of secondary toxins as it produces carbon dioxide (CO_2) and water (H_2O) [6]. In the process of photocatalysis, superoxide anion and hydroxyl radical generation will attack organic compounds in the wastewater in the presence of light of appropriate wavelengths. These organic compounds can be degraded into non-hazardous compounds [7].

Among other semiconductors, such as zinc oxide and copper oxide in photocatalysis, TiO_2 has promising potential. Chemical stability, low cost, reusability, and chemical inertness are some of the advantages of TiO_2 [8–10]. TiO_2 occurs in three crystalline forms, which are anatase, rutile, and brookite. These all have large band gaps, with values of 3.2 and 3.0 eV being reported for anatase and rutile, respectively, whereas the corresponding value for brookite is scarcely reported due to processing difficulties [11, 12]. However, a few studies have reported that the band gap values of brookite range from 3.1 to 3.4 eV [13]. Rutile has a more thermodynamically stable phase and smaller band gap compared to anatase [14]. However, the anatase phase has superior photocatalytic behaviour compared to rutile [15, 16]. The origin of the low photocatalytic activity of the TiO_2 rutile phase may be due to its low surface area resulting from the synthesis route that induces aggregation by thermal treatment at high temperatures (400–1000 °C) [17]. Moreover, the main active facet of rutile is (110) which has a low surface energy that hinders the adsorption and degradation of molecules [18]. Hence, fabricating TiO_2 with high-activity facets is very challenging.

Numerous methods have been reported for the fabrication of TiO_2 film, such as spray pyrolysis [19], hydrothermal [20], spin coating [21], and so on. Among these methods, a simple, fast, energy-saving and cost-effective low-temperature hydrothermal method is easily adjusted to the TiO_2 morphology with a homogeneous film distribution system [22]. By using the low-temperature hydrothermal process, the rutile phase can be formed without additional thermal treatment [23]. In recent decades, various TiO_2 morphologies such as wires, rods, flower-like, and tubes have been developed [24]. Hydrothermal synthesis with acidic solution has the ability to produce a rutile-phase TiO_2 flowerlike structure [25]. The flowerlike structure with stacking growth helps to increase surface area during growth [26]. The three-dimensional flowerlike structure not only reflects light many times, but also improves the amount of incident light dispersion for best light harvesting to enhance the photocatalytic performance compared to 1D nanorod structures [27–29]. The numerous petals of the flowerlike structure also have more active sites for photocatalysis. Moreover, a solid film can be formed with the formation of a flowerlike rutile-phase structure on top of a fluorine-doped tin oxide (FTO) substrate [26]. Immobilisation of the catalyst will avoid the need for any post-

Table 1 Comparison of studies of TiO_2 film for MB degradation

Synthesis method	Phase type	Percentage degradation (%)	Degradation duration (minutes)	Ref
DC reactive magnetron sputtering	Mixed phase	30	40	[57]
Dip-coating technique	Anatase	100	480	[58]
Ball milling	Rutile	64	540	[59]
Hydrothermal method	Rutile	38	180	[60–62]
Hydrothermal method	Rutile	60	300	This study

separation processes between the catalyst and treated wastewater [30, 31], and prevent excessive solids from seeping into the water stream that can be detrimental to aquatic life.

The efficiency of photocatalysis is strongly dependent on the number of operating parameters that control the photodegradation of the organic molecule. Photocatalytic degradation of coloured dyes such as MB is affected by a number of parameters, such as the initial solution pH, catalytic morphology, presence of oxygen vacancy/Ti^{3+} surface defects, and the initial concentration of MB. The surface charge properties of TiO_2 are also dependent on pH change due to the amphoteric behaviour of the TiO_2 semiconductor [32]. According to Ling et al. [33], electrostatic interactions between negative TiO^- surface sites and methylene blue cations under basic conditions lead to strong adsorption with correspondingly high degradation rates. Hamed et al. [30] claimed that the photocatalytic degradation of MB is significantly influenced by electron trapping which occurs in the presence of oxygen vacancy/Ti^{3+} surface defects that can prolong the lifetime of electrons and holes. Zhang et al. [11] claimed that the anatase phase has a better photocatalytic activity compared to the rutile phase due to anatase having a higher surface adsorption and lower recombination rate than rutile. Lin et al. [31] claimed that bicrystalline TiO_2 has excellent interface contact and optimised band structure which enhances photocatalytic activity. However, the fabrication of a bicrystalline material with controlled anatase and rutile proportions is complex [31]. Feng et al. [34] discovered that rutile (110) and (111) exposed facets can enhance the separation of electrons and holes that can improve the photocatalytic activity. These studies show that there is still controversy in the literature around optimising the photocatalytic activity of the rutile phase TiO_2 films that can have a major impact on photocatalytic activity and degradation of organic wastes.

The aim of this study was to enhance the photocatalytic activity of the rutile phase. Thus, several precursor concentrations were used to develop a flowerlike rutile-phase TiO_2 film via a low-temperature hydrothermal method. The remarkable activity of the resulting material with (101) active facets is discussed, including the impact on MB photodegradation of process parameters such as morphology, active surface species, initial concentration of MB, and solution pH. The reusability of the film, the possible formation of flowerlike rutile-phase TiO_2, and the mechanism for photocatalytic degradation of MB are also discussed in this paper. Even though TiO_2 is a common photocatalyst, the fabrication method and research results in this work have important reference values in the photocatalytic field. Table 1 shows a summary of previous studies on TiO_2 films used for photocatalytic MB degradation. It can be seen that the flowerlike rutile-phase TiO_2 film produced in this work showed excellent photocatalytic activity compared to alternative rutile or mixed-phase materials.

2 Experimental method

2.1 Materials

Hydrochloric acid (HCl) was obtained from JT Baker with 36–38% purity. Titanium (IV) butoxide (TBOT) and FTO-coated glass substrates were purchased from Sigma Aldrich. Methylene blue (MB), benzoic acid, potassium persulfate, and disodium ethylenediaminetetraacetate (EDTA–2Na) were obtained from Wako. All chemicals were used without any purification.

2.2 Preparation of flowerlike rutile-phase TiO_2 film

Rutile-phase TiO_2 film was fabricated by using a simple hydrothermal method. The FTO substrate was cut into sections with dimensions of 35 × 35 mm and subsequently cleaned with acetone, ethanol, and deionised (DI) water with sonication. Next, 80 mL of HCl (0.016 M) was mixed with 80 mL of DI water and stirred for 5 min. TBOT was then added dropwise to achieve overall Ti(IV) concentrations of 0.05 to 0.15 M and stirred until the solution was clear. The FTO substrate (conducting surface upwards) was placed in a Teflon-lined hydrothermal autoclave (300 mL). Then, the prepared TiO_2 solution was poured into the autoclave and placed into an oven for 10 h at 150 °C. Figure 1a shows the illustration of the Teflon-lined hydrothermal autoclave. After cooling, the prepared film was washed several times in DI water and dried in the oven for 30 min at 100 °C. The films were labelled as T-0.05 M,

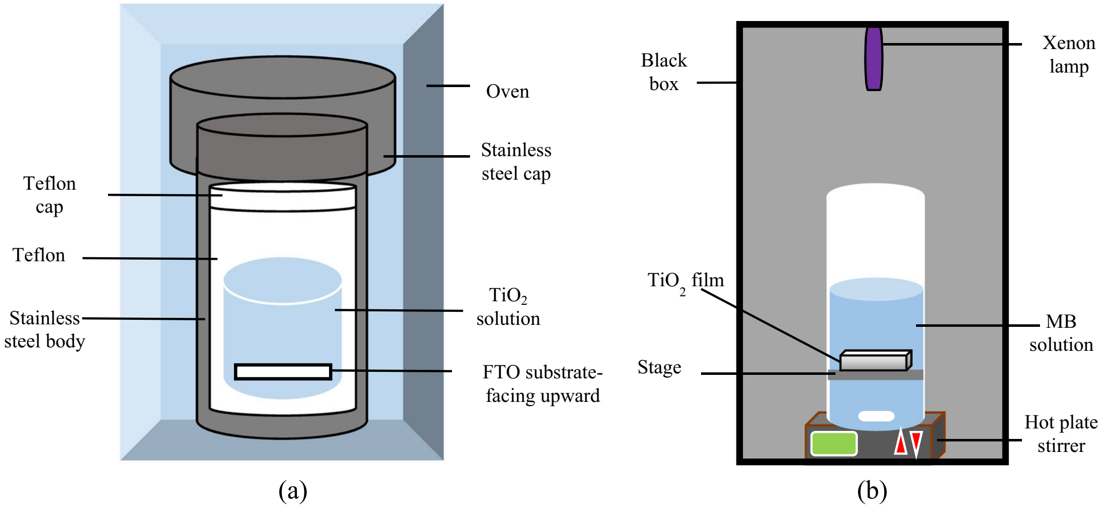

Fig. 1 **a** Hydrothermal processing of flowerlike rutile films, **b** schematic illustration of the photocatalytic reactor used

T-0.07 M, T-0.10 M, T-0.12 M, and T-0.15 M according to the precursor molarities used for each sample.

2.3 Characterisations

For X-ray diffraction (XRD), PANalytical X'Pert Powder at 2θ angles from 20° to 80° was used to investigate the crystal structure of the TiO_2 films. Raman spectroscopy (Xplora plus model BX41TF) was used to confirm the structural property of the rutile-phase TiO_2 film. Scanning electron microscopy (SEM; JEOL JSM-7600 F) was used to analyse the surface morphology of the samples. Transmission electron microscopy (TEM; JEOL JEM 2100 F) with accelerating voltage of 200 kV was used to observe the crystallite size and obtain high-resolution images of the films. The defect state of the TiO_2 samples was investigated via photoluminescence spectroscopy (Jasco spectrofluorometer FP-8600). UV–vis DRS spectroscopy (SHIMADZU UV 3600 plus) was used to examine the optical properties of the films. XPS (SHIMADZU AXIS ULTRA DXD) was utilised to investigate the chemical state of surface species in the films.

2.4 Photodegradation of MB

The photocatalytic activity of the TiO_2 films was tested via MB degradation using a xenon lamp (300 W) operating over a broad wavelength range (300–600 nm) and located 21 cm from the photocatalyst. The TiO_2 film was placed in a beaker. Then, the film was exposed to light for 30 min to remove any contamination on top of the TiO_2 surface to improve the adsorption of MB. Then, 100 mL of MB solution was poured and stirred under dark conditions for 1 h to achieve adsorption–desorption equilibrium. The initial pH of the solution was 8. Subsequently, photocatalytic experiments were carried out for 5 h with continuous stirring. MB solution (3 mL) was collected at 1 h intervals. For exploring the effects of pH, the pH was varied from 3 to 12. Hydrochloric acid (HCl) or sodium hydroxide (NaOH) was used to adjust the pH as required. EDTA–2NA was used as the scavenger for superoxide anions, potassium persulfate as the scavenger for hole ions, and benzoic acid as the scavenger for hydroxyl radicals. For scavenging analysis, sufficient scavenger was added to the 100 mL MB solution to achieve a scavenger concentration of 1 mM. Figure 1b illustrates the photocatalysis reactor for the experiment. The reusability experiment was carried out using the T-0.10 M film to study the stability of the film after 5 runs with 5 ppm concentration of MB with the same TiO_2 film. The dye degradation was calculated by using Eq. (1):

$$\text{Dye degradation}\,(\%) = (A_o - A_t/A_o) \times 100 \tag{1}$$

where A_o is initial absorbance and A_t is absorbance at time t. The absorbance of MB was read at 664 nm.

3 Results and discussion

3.1 Crystallinity and chemical state of TiO_2 film

The XRD patterns of TiO_2 films prepared using different TBOT concentrations are shown in Fig. 2a. The XRD patterns demonstrate that the hydrothermal synthesis results in the creation of pure rutile-phase TiO_2 (JCPDS file no. 98-008-0842) without the need for subsequent calcination. The peaks observed at 2θ values of 27.38°, 36.10°, 41.24°, and 54.32° are well matched to the (110), (101), (111), and

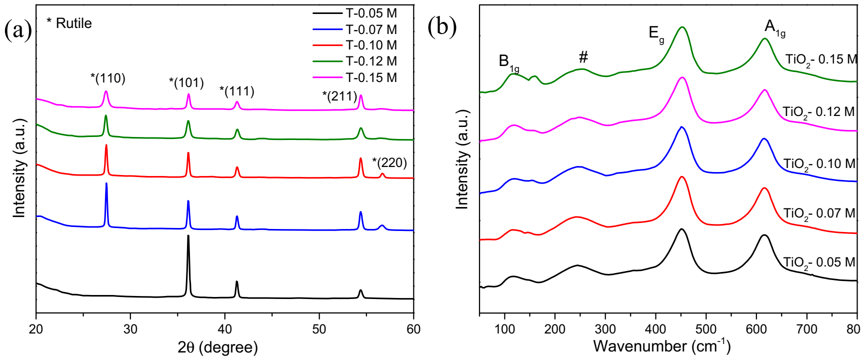

Fig. 2 **a** XRD patterns and **b** Raman spectra of films obtained using different concentrations of TBOT

(211) planes, respectively, of rutile TiO_2 [35, 36], demonstrating the polycrystalline nature of the sample. The removal of the calcination step prior to the formation of the rutile-phase may prevent the possibility of morphological damage to the surface, leading to a reduction in the active surface region. The similar lattice structures of FTO and TiO_2 also helps to provide growth sites for rutile-phase TiO_2 without the assistance of a rutile seed layer of TiO_2, since the TiO_2 rutile-phase has a tetragonal structure similar to that of FTO (FTO: $a = b = 0.4687$ nm; rutile: $a = b = 0.4594$ nm) [37]. At a precursor concentration of 0.05 M, the film exhibited preferential (101) orientation, with no flowerlike structure being obtained (see below) [35].

Using the Debye–Scherrer equation with the major peak of the rutile phase at $2\theta = 27.38°$, the crystallite size of rutile-phase TiO_2 was determined as follows:

$$D = k\lambda/\beta\cos\theta \tag{2}$$

where D is the crystallite size, k is the shape factor ($k = 0.94$), λ is the wavelength of the X-ray radiation (Cu $K\alpha = 0.1542$ nm), β is full-width at half-maximum (FWHM), and θ is the angular position of the diffraction peaks.

The measured FWHM, crystallite size, lattice strain and d-spacing obtained at different TBOT concentrations are shown in Table 2. The findings indicate that as the TBOT concentration increased, the crystallite size decreased. This result is in line with the analyses by Tran et al. [36], where the exposed rutile (110) plane appears to have a larger surface area. The increased FHWM value indicated a decrease in the crystallite size, the increasing FWHM value may also be influenced by lattice strain in the TiO_2. The lattice strain of the sample was estimated by using the Williamson–Hall relation [38]:

$$\beta\cos\theta = 4\varepsilon\sin\theta + \frac{k\lambda}{D} \tag{3}$$

from the slope of β cos θ vs 4 sin θ. Here, D and ε are the average crystallite size and lattice strain, respectively. As shown in Table 2, the lattice strain decreased with increasing precursor solution concentration from 0.07 to 0.10 M and then increased with further increases in TBOT concentration, due presumably to differences in the density of intrinsic defects (such as Ti^{4+} and/or F^+ oxygen vacancy defects) in the samples [39]. These results suggest that a TBOT precursor concentration of 0.10 M may be optimal for controlling the growth of rutile-phase TiO_2 films under the conditions used in this study.

Table 2 FWHM, crystallite size, lattice strain, and *d*-spacing of films obtained using different TBOT concentrations

Sample	β (FWHM)	D (nm)	Lattice strain	d-spacing (Å)
0.07 M	0.1476	116	0.00204	3.2502
0.10 M	0.1968	87	0.00108	3.2525
0.12 M	0.2952	58	0.00281	3.2556
0.15 M	0.492	35	0.00427	3.2560

The Raman spectra obtained from the films are also consistent with the formation of pure rutile-phase TiO_2 (Fig. 2b). The spectra all exhibit three well-defined bands at 116, 453, and 617 cm^{-1}, which are associated with the rutile-phase TiO_2 [40], consistent with the XRD patterns (although it must be noted that Raman spectroscopy probes short-range order whereas XRD probes long-range order). No peaks attributable to anatase or brookite are evident. The key Raman modes are assigned as follows: 116 cm^{-1} (O–Ti–O symmetric bending vibration, B_{1g}); 244 cm^{-1} (multi-phonon process); 453 cm^{-1} (O–Ti–O symmetric stretching vibration, E_g); and 617 cm^{-1} (O–Ti–O antisymmetric bending vibration, A_{1g}) [41].

The XPS spectra of T-0.1M (with binding energies references to that of C 1*s*) clearly reveal the presence of Ti^{3+} surface sites (Fig. 3). The Ti 2*p* appears as a doublet, with a splitting of 5.7 eV (Fig. 3a). Band fitting revealed that the Ti 2*p* profile consisted of four peaks attributed to Ti^{4+} (major components, 460.2 and 465.9 eV) and Ti^{3+} (shoulders at 459 and 464.8 eV) [42], consistent with the presence of Ti^{3+} surface defects in the film. In order to boost the photocatalytic activity of rutile, (111) and (110) facets is important because this facet will act as the oxidative and reductive site [43].

With the co-existence of Ti^{3+} in the flowerlike rutile-phase TiO_2, the photocatalytic efficiency of rutile TiO_2 can be further enhanced by increasing the separation of photogenerated electron–holes, thereby limiting the rate of recombination.

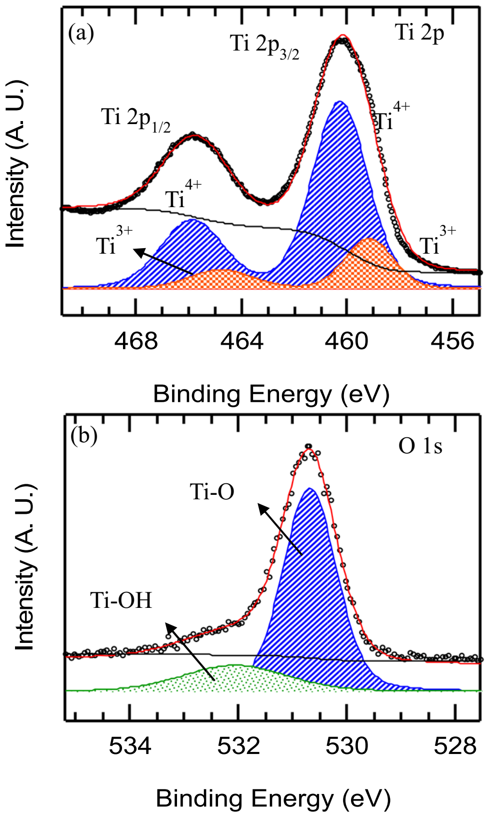

Fig. 3 XPS spectra of T-0.10 M: **a** Ti 2*p* and **b** O1*s*

3.2 Morphology of TiO_2 Film

FESEM and HR-TEM were used to examine the morphology of the TiO_2 films. Figure 4 shows significant morphological dependence of TiO_2 synthesised using different TBOT concentrations. The TiO_2 film deposited using the 0.05 M TBOT precursor was composed of oriented rod-like crystallites with a mean height of 3.28 µm. A flowerlike structure appearing at the top of the rods with a mean height of 19.8 µm at 0.07 M TBOT precursor. As the TBOT concentration was increased to the optimum concentration (0.10 M), a clearer growth of more petals was observed due to the rapid development of TiO_2 flowers stacked on each other with maximum coverage of the rod. The height of the rods and the flowers was 33.9 µm. Further increases in TBOT concentration led to a reduction in the height of the rods and flowers and disrupted the flowerlike structure. As TBOT concentration was increased to above the optimal concentration, competition between adjacent rods for the available precursor increased and impeded the growth of TiO_2 [32].

The microstructure of the T-0.10 M sample was further investigated using HR-TEM. Figure 5a–c shows that there was a bundle of single nanorods in each petal of the flowers observed in the FESEM images, which was in the range of 90–200 nm. The nanorods were approximately 7 nm in size. These nanorods appeared to bond together in a particular direction to form the microrod petals for the flowerlike structure. The tip of the rods had a prismatic shape with (101) facets as shown in Fig. 5c. The polycrystalline structure was revealed in the bulk of the rods in Fig. 5d. The *d*-spacing values for planes (110), (101), (111), and (211) are 3.25, 2.48, 2.18, and 1.68 Å, respectively. These values agree well with the results obtained via XRD. The different

Fig. 4 FESEM images of films deposited using different TBOT concentrations. Top view: **a** T-0.05 M, **b** T-0.07 M, **c** T-0.10 M, **d** T-0.12 M, **e** T-0.15 M. Cross-section view: **f** T-0.05 M, **g** T-0.07 M, **h** T-0.10 M, **i** T-0.12 M, **j** T-0.15 M

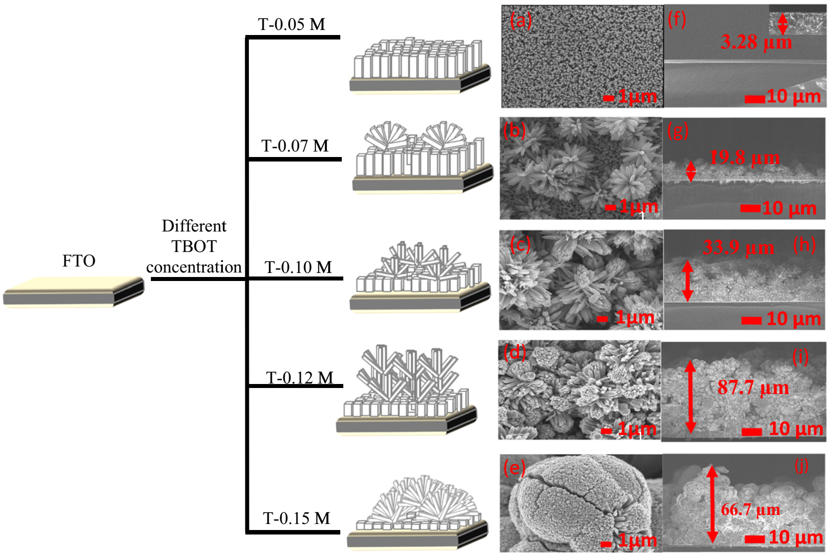

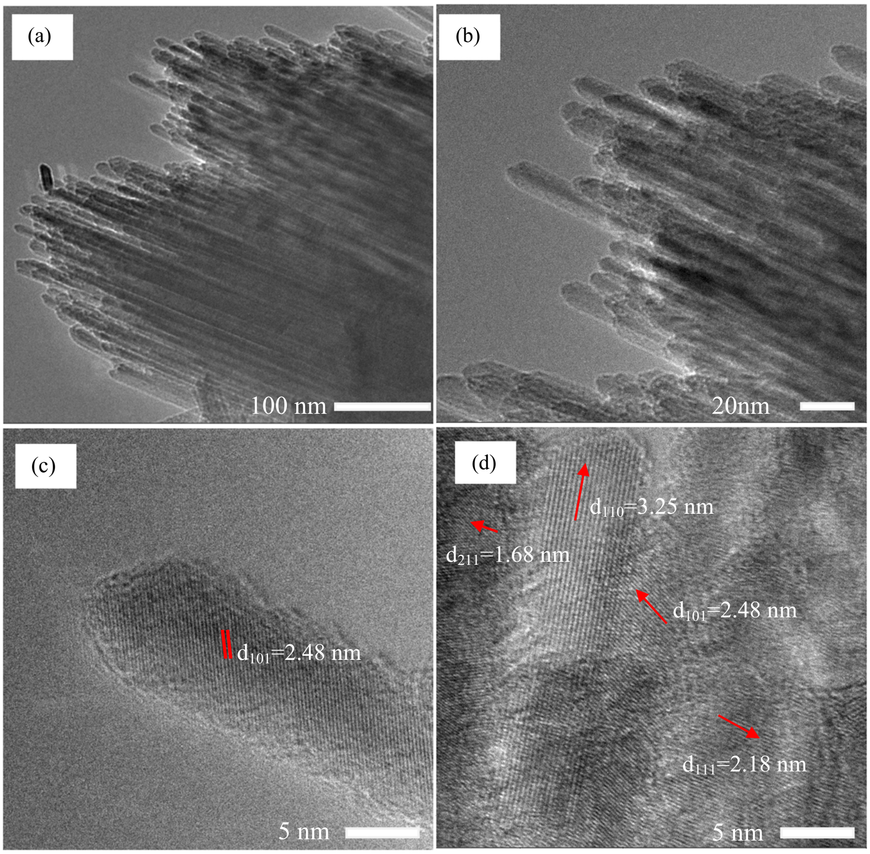

Fig. 5 TEM images of T-0.10 M at different magnifications **a** 50K magnification **b** 200K magnification **c** 600K magnification (tip) **d** 600K (bulk)

samples also underwent wettability analysis. Fig. S1 shows the wettability properties for films deposited using different concentrations of titanium precursors. The different morphologies lead to differences in the wettability of the films. The details are provided in the Supplementary Information.

3.3 Optical properties of TiO_2 film

The reflectance of the material was investigated with UV–vis reflectance spectroscopy. Figure 6a shows that all the samples have good absorbance properties in the UV region. The reflectance of the light in the UV region decreased with increased TBOT concentration. The band gaps were determined using Tauc plots to be 3.36, 3.31, 3.21, 3.12, and 3.06 eV for T-0.05 M, T-0.07 M, T-0.10 M, T-0.12 M, and T-0.15 M, respectively, as shown in Fig. 6b–f. When the TiO_2 film was exposed to light, the Ti^{3+} and oxygen vacancy defect formed a mid-gap state [44]. From the dependence of the band gap on film thickness, it can also be clarified that the band gap energy decreases as film thickness increases. This may be due to increased TiO_2 film surface area, in which more electrons and holes were created when the film is thicker [45].

Figure 7 presents the photoluminescence spectrum for the T-0.10 M sample. In order to investigate electron recombination in the UV spectrum and visible spectrum, the excitation wavelength was set at 320, 420, and 500 nm. The three major levels inside the band gap at 320 nm (UV spectrum) consist of self-trap excitation, surface state and oxygen vacancy, and Ti^{3+} [46]. Emissions peaked at approximately 2.94, 2.74, 2.65, 2.57, 2.52 and 2.06 eV (Fig. 7a). The surface-state emission induces other emission peaks. The surface state is a shallow trap situated within the catalyst's band gap near the absorption band edge and functions as an electron trap that can induce an emission at a higher wavelength [47]. The oxygen vacancy-Ti^{3+} surface defect condition, which is located at about 0.7 eV below the conduction band, is responsible for the emission peak at 2.06 eV [48, 49]. This state is created by transferring the electron in an oxygen vacancy to the adjacent Ti atom [50]. Emissions in the visible region are triggered by the recombination of the electron and hole at the oxygen vacancy-Ti^{3+} surface defect state. This state traps the electron, thus inhibiting recombination with the hole. Two emission peaks at 455 and 534 nm were observed under 420 nm excitation. Even though the excitation wavelength was less than the band gap energy of the TiO_2 sample, a strong emission peak was observed at 455 nm (2.72 eV). This outcome is attributed to the photo-excited electron falling into oxygen vacancy-Ti^{3+} surface defect states under the band gap energy [50].

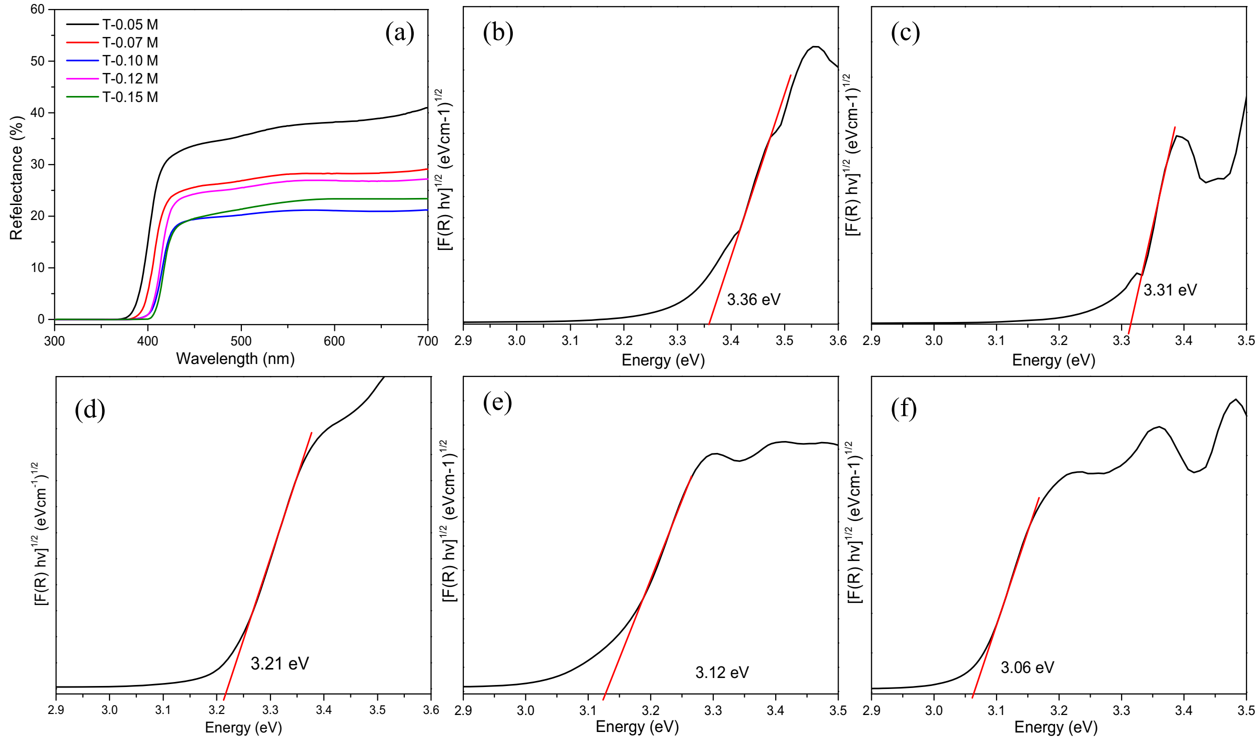

Fig. 6 **a** Reflectance spectra, and Tauc plots for **b** T-0.05 M, **c** T-0.07 M, **d** T-0.10 M, **e** T-0.12 M, **f** T-0.15 M

Fig. 7 Photoluminescence spectra for T-0.10 M film at different excitation energy: **a** 325 nm and **b** 420 nm

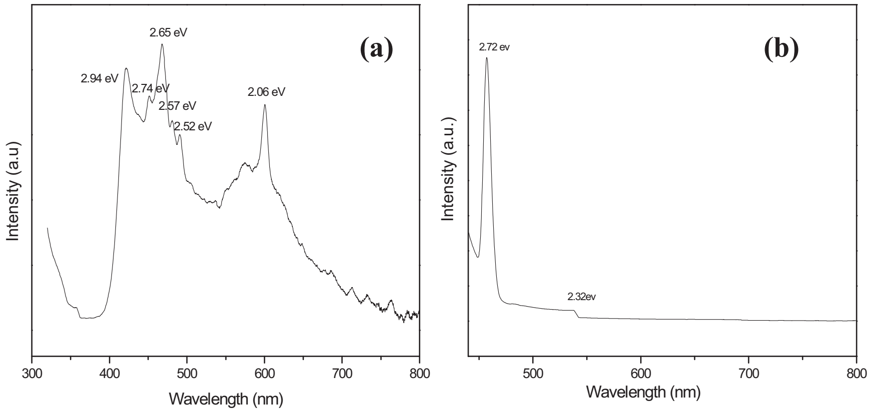

3.4 Photodegradation of MB

For MB degradation, the efficiency the TiO_2 films made using different TBOT concentrations was investigated. The MB solution had an initial pH of 8 and the MB concentration was 5 ppm. An experiment without TiO_2 film (photolysis) was also performed in the presence of light irradiation. The result shows only 18% photolysis degradation occurred, while T-0.10 M film obtained a maximum of 42% dye degradation, followed by T-0.15 M with 37%, T-0.12 M with 35%, T-0.07 M with 28%, and T-0.05 M with 25% for 5 h of photodegradation. Compared to powder catalysts, the dye degradation using the TiO_2 films was less efficient, but post-separation after treatment resulted in a more beneficial and cost-effective treatment. A summary of the percentage of dye degradation for films prepared using different TBOT concentrations is shown in Fig. 8a. These findings can be explained by the fact that in dye degradation, oxygen vacancy and Ti^{3+} defect play a significant role. A shallow trap was introduced by this defect that could inhibit electron and hole recombination [47]. Surface area and crystallinity are other key factors. The rods inside the flowers had a major effect that contributed to the dispersion of light, allowing the incident light to be scattered and more effectively absorbed and utilised within the film and be absorbed during the photocatalytic process [51], thus enhancing the mobility of the electrons in the TiO_2 film [52]. The stack effect creates a gap between the structural

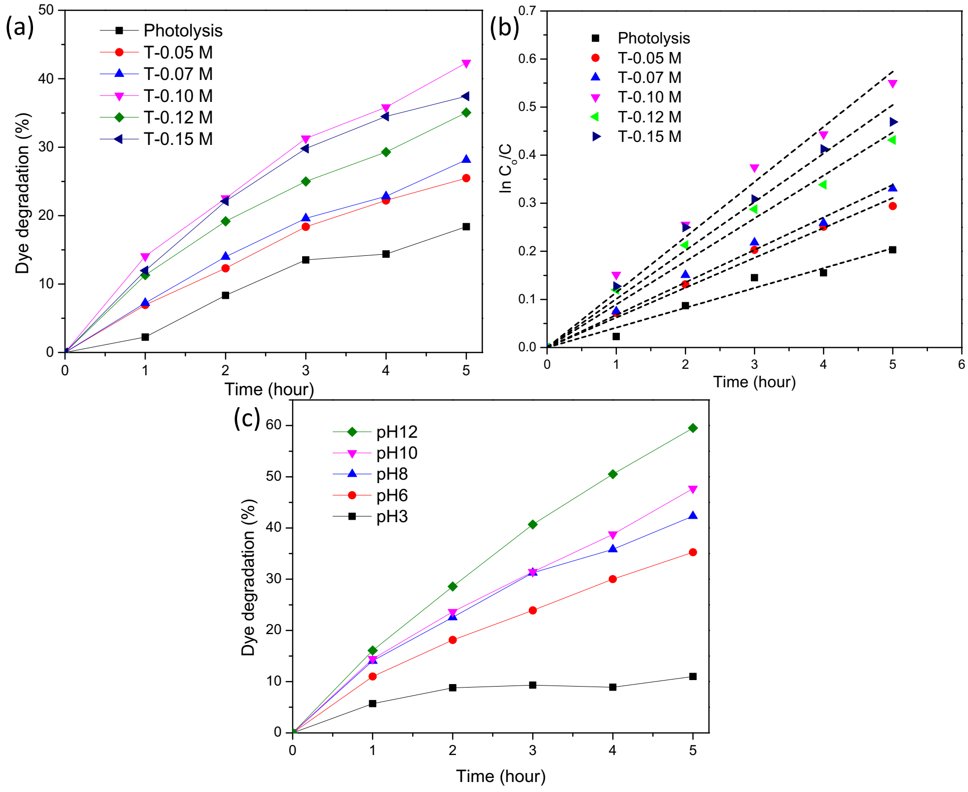

Fig. 8 Dye degradation percentage over time with **a** different morphologies, (b) ln (C_0/C_t) vs time, **c** different pH by using T-0.10 M film

components of the flowers and provides a path for water to diffuse within the film while providing more active areas between surface TiO_2 and wastewater for photocatalytic action. These factors are consistent with previous studies [15]. The kinetic analysis of the effect of different TBOT concentrations on their photocatalytic behaviour was conducted with the assistance of broad-spectrum irradiation. The Langmuir–Hinshelwood (L–H) model was used to analyse the kinetic rate of heterogeneous photocatalysis for the degradation of an organic compound [53]. The L–H model formula is expressed in Eq. (3):

$$\ln\frac{C_0}{C_t} = K_{app}t \tag{4}$$

where C_0 and C_t are the dye degradation at time 0 and time t, respectively, while k_{app} is the apparent pseudo-first-order rate constant.

Figure 8b shows the graph ln (C_0/C_t) vs irradiation period for MB degradation using various catalysts, confirming that the pseudo-first-order was followed by the reactions. As shown in Table 3, the maximum rate constant was observed for the T-0.10 M film ($K_{app} = 0.183 \times 10^{-2}\ \text{min}^{-1}$), with decreasing rate constants evident for the films produced at higher and lower TBOT concentrations. This data can be correlated with the FESEM images (Fig. 4) which showed that the open flowerlike structure progressively formed as the TBOT concentration was increased from 0.05 to 0.1 M was then transformed into a more tightly packed cauliflower-like morphology with further increases in TBOT concentration.

Table 3 Dye degradation and kapp value for various samples

		Dye degradation after 5 h (%)	K_{app} ($\times 10^{-2}$ min^{-1})	R^2 value
TBOT concentration (M)	Photolysis	18	0.001	0.964
	0.05	25	0.098	0.996
	0.07	28	0.110	0.997
	0.10	42	0.183	0.994
	0.12	35	0.143	0.992
	0.15	37	0.156	0.990

The optimum rutile film (T-0.10 M) was further studied for important parameters affecting MB photodegradation, such as MB concentration, pH, active species, and film reusability. Another important parameter in photocatalytic behaviour is pH. The pH determines the photocatalyst's surface charge. When the solution's pH is at or below the isoelectric point, adsorption of the dye is minimal; the photocatalyst surface is charged positively below the isoelectric point and retains a negative charge above it [54]. In analysing the surface charge of rutile-phase TiO_2, the pH ranges were set from acidic to alkaline. The dye degradation at different pH is shown in Fig. 8c. At pH 12, the degradation increased to 60%, while the lowest degradation was 11% at pH 3. This phenomenon is explained by the amphoteric behaviour of the rutile-phase TiO_2 film during the reaction. Jalil et al. reported that for rutile-phase TiO_2, the point of zero charge (pH_{zpc}) is pH 6 [55]. Uptake of the (positively charged) MB is also enhanced at pH greater than the pH_{zpc} [56]. This result is consistent with those reported by Ling et al., who noted that the electrostatic interaction between negative TiO^- and MB cations contributes to a fast degradation rate due to strong adsorption of the dye [33]. The effects of MB concentration, active species analysis and reusability analysis for the flowerlike rutile-phase TiO_2 films were also analysed; further details are provided in Supplementary information.

4 Conclusion

Rutile-phase TiO_2 films with a flowerlike morphology were successfully fabricated on FTO substrates by using a hydrothermal method. To obtain the optimised flowerlike morphology, the Ti(IV) concentration in the precursor solutions used to deposit the films was varied. Under all conditions used in this study, the TiO_2 films obtained consisted of a pure rutile-phase, as shown by Raman spectroscopy and XRD analysis. The flowerlike morphology was transformed into a cauliflower-like morphology as the precursor concentration increased. PL and XPS analysis confirmed the existence of Ti^{3+} and oxygen vacancy defects in the optimised coating.

It was shown that films obtained from precursor solutions containing 0.10 M Ti(IV) has the highest MB degradation (42% over 5 h), which is attributed to the intriguing flowerlike morphology of the film, together with the presence of oxygen vacancy/Ti^{3+} surface defect sites. Furthermore, the presence of Ti^{3+} surface defect and oxygen vacancy introduced the shallow level, which helped to trap photogenerated electrons and prolong the lifetime of the electron/hole pair that mediates dye degradation. The MB degradation was further improved up to 60% at pH 12 at 5 ppm MB concentration, due to electrostatic interactions between the negatively charged TiO_2 surface and MB cation which enhanced the uptake of MB on the surface of the photocatalyst. Of the active species potentially contributing to the photocatalytic activity, hydroxyl radicals were identified as the most significant based on scavenging studies. The reusability of the optimised photocatalyst was tested, demonstrating that it retained around 90% of its initial activity even after five cycles.

The flowerlike rutile-phase TiO_2 film has significant potential to enhance conventional approaches used in industrial wastewater treatment.

Acknowledgements The authors would like to thank the Ministry of Higher Education for the financial support under the Fundamental Research Grant Scheme (FRGS) number: FRGS/1/2020/STG05/UTHM/02/4. The authors would also like to thank the Centre for Instrumental Analysis, Shizuoka University, Hamamatsu, Japan for the characterisation equipment.

Author contribution N.K.A.H.: investigation and writing—original draft. M.K.A.: conceptualisation and supervision. N.H.H.H.: formal analysis and validation. A.B.F.: writing—review and editing and resources. A.B.S. and S.M.M.: conceptualisation and methodology. M.H.M.: writing—review and editing, and validation. M.S.: conceptualisation and supervision. F.I.M.F.: conceptualisation. A.M.: writing—editing. A.M.: validation. M.F.M.S.: writing—review.

Compliance with ethical standards

Conflict of interest The authors declare no competing interests.

Ethical approval This article does not contain any studies with human participants or animals performed by any of the authors.

Publisher's note Springer Nature remains neutral with regard to jurisdictional claims in published maps and institutional affiliations.

References

1. Arora C, Soni S, Sahu S et al. (2019) Iron based metal organic framework for efficient removal of methylene blue dye from industrial waste. J Mol Liq 284:343–352. https://doi.org/10.1016/j.molliq.2019.04.012
2. Eljiedi AAA, Kamari A (2017) Removal of methyl orange and methylene blue dyes from aqueous solution using lala clam (Orbicularia orbiculata) shell. AIP Conf Proc 1847:40003. https://doi.org/10.1063/1.4983899
3. Taylor P, Hanis N, Hairom H et al. (2014) Utilization of self-synthesized ZnO nanoparticles in MPR for industrial dye wastewater treatment using NF and UF membrane. Desalin Water Treat 37–41. https://doi.org/10.1080/19443994.2014.917988
4. Akpan UG, Hameed BH (2009) Parameters affecting the photocatalytic degradation of dyes using TiO_2-based photocatalysts: a review. Hazard Mater 170:520–529. https://doi.org/10.1016/j.jhazmat.2009.05.039
5. Shoabargh, S. Karimi A, Dehghanb G, Khataee A (2016) A hybrid photocatalytic and enzymatic process using glucose oxidase immobilized on TiO_2/polyurethane for removal of a dye. Ind Eng Chem Res 2–9. https://doi.org/10.1016/j.jiec.2013.11.058
6. Arabatzis IM, Antonaraki S, Stergiopoulos T et al. (2002) Preparation, characterization and photocatalytic activity of nanocrystalline thin film TiO_2 catalysts towards 3,5-dichlorophenol degradation. J Photochem Photobiol A Chem 149:237–245. https://doi.org/10.1016/S1010-6030(01)00645-1
7. Hanis N, Hairom H, Wahab A et al. (2015) Influence of zinc oxide nanoparticles in the nanofiltration of hazardous Congo red dyes. Chem Eng J 260:907–915. https://doi.org/10.1016/j.cej.2014.08.068
8. Dong H, Zeng G, Tang L et al. (2015) An overview on limitations of TiO_2-based particles for photocatalytic degradation of organic pollutants and the corresponding countermeasures. Water Res 79:128–146. https://doi.org/10.1016/j.watres.2015.04.038
9. Park JH, Kim S, Bard AJ (2006) Novel carbon-doped TiO_2 nanotube arrays with high aspect ratios for efficient solar water splitting. Nano Lett 6:24–28. https://doi.org/10.1021/nl051807y
10. Tao Y, Han Z, Cheng Z et al. (2015) Synthesis of nanostructured TiO_2 photocatalyst with ultrasonication at low temperature Journal of Materials Science and Chemical Engineering 3:29–36

11. Zhang J, Zhou P, Liu J, Yu J (2014) New understanding of the difference of photocatalytic activity among anatase, rutile and brookite TiO_2. Phys Chem Chem Phys 16:20382–20386. https://doi.org/10.1039/c4cp02201g
12. Zhao B, Zhou J, Chen Y, Peng Y (2011) Effect of annealing temperature on the structure and optical properties of sputtered TiO_2 films. J Alloys Compd 509:4060–4064. https://doi.org/10.1016/j.jallcom.2011.01.020
13. Monai M, Montini T, Fornasiero P (2017) Brookite: nothing new under the Sun? Catalysts 7:1–19. https://doi.org/10.3390/catal7100304
14. Qian X, Han H, Chen Y, Yuan Y (2018) Sol–gel solvothermal route to synthesize anatase/brookite/rutile TiO_2 nanocomposites with highly photocatalytic activity. J Sol-Gel Sci Technol 85:394–401. https://doi.org/10.1007/s10971-017-4544-3
15. Ramirez-Sant A, Acevedo-Peña P, Córdoba EM (2012) Enhanced photocatalytic activity of TiO_2 film by modification with polyethylene glycol Quim Nov 35:1931–1935
16. Sabry RS, Muhsin YKA (2016) Synthesis and photocatalytic activity of TiO_2 nanoparticles prepared by sol–gel method. J Sol-Gel Sci Technol 78:299–306. https://doi.org/10.1007/s10971-015-3949-0
17. Jung HS, Kim H (2009) Origin of low photocatalytic activity of Rutile TiO_2. Electron Mater Lett 5:73–76. https://doi.org/10.3365/eml.2009.06.073
18. Zhang J, Liu P, Lu Z et al. (2015) One-step synthesis of rutile nano-TiO_2 with exposed {111} facets for high photocatalytic activity. J Alloy Compd J 632:133–139. https://doi.org/10.1016/j.jallcom.2015.01.170
19. Kamalia N, Hamed A, Mahat R et al. (2016) Dye-sensitized solar cell using spray pyrolysis deposition method. Journal of Engineering and Applied Sciences 11:8846–8851
20. Hamed NKA (2016) Influence of hydrochloric acid volume on the growth of titanium dioxide (TiO_2) nanostructures by hydrothermal method. Sains Malaysiana 45:1669–1673
21. Lee DY, Kim JT, Park JH et al. (2013) Effect of Er doping on optical band gap energy of TiO_2 thin films prepared by spin coating. Curr Appl Phys 13:1301–1305. https://doi.org/10.1016/j.cap.2013.03.025
22. Shinde DB, Jagadale SK, Mane RK, Mane RM, Ghanwat VB (2015) Time dependent facile hydrothermal synthesis of TiO_2 nanorods and their photoelectrochemical applications J Nanomed Nanotechnol S7:004. https://doi.org/10.4172/2157-7439.S7-004
23. Zhao Z, Zhang X, Zhang G et al. (2015) Effect of defects on photocatalytic activity of rutile TiO_2 nanorods. Nano Res 8:4061–4071. https://doi.org/10.1007/s12274-015-0917-5
24. Savage N, Diallo MS (2005) Nanomaterials and water purification: opportunities and challenges. J Nanoparticle Res 7:331–342. https://doi.org/10.1007/s11051-005-7523-5
25. Jordan V, Javornik U, Plavec J et al. (2016) Self-assembly of multilevel branched rutile-type TiO_2 structures via oriented lateral and twin attachment. Sci Rep 6:1–13. https://doi.org/10.1038/srep24216
26. Ye M, Liu H-Y, Lin C, Lin Z (2013) Hierarchical rutile TiO_2 flower cluster-based high efficiency dye-sensitized solar cells via direct hydrothermal growth on conducting substrates. Small 9:312–321. https://doi.org/10.1002/smll.201201590
27. Lazar MA, Varghese S, Nair SS (2012) Photocatalytic water treatment by titanium dioxide: recent updates. Catalyst 2:572–601. https://doi.org/10.3390/catal2040572
28. Wu G, Wang J, Thomas DF, Chen A (2008) Synthesis of F-doped flower-like TiO_2 nanostructures with high photoelectrochemical activity. Langmuir 24:3503–3509
29. Rashid SA (2010) Immobilisation of titanium dioxide onto supporting materials in heterogeneous photocatalysis: A review. Appl Catal A Gen 389:1–8. https://doi.org/10.1016/j.apcata.2010.08.053
30. Hamed NKA, Ahmad MK, Hairom NHH et al. (2020) Dependence of photocatalysis on electron trapping in Ag-doped flowerlike rutile-phase TiO_2 film by facile hydrothermal method. Appl Surf Sci 534:147571. https://doi.org/10.1016/j.apsusc.2020.147571
31. Lin X, Sun M, Gao B et al. (2021) Hydrothermally regulating phase composition of TiO_2 nanocrystals toward high photocatalytic activity. J Alloys Compd 850:156653. https://doi.org/10.1016/j.jallcom.2020.156653
32. Mamun K, Asw R, Fahmida K (2017) Parameters affecting the photocatalytic degradation of dyes using TiO_2: a review. Appl Water Sci 7:1569–1578. https://doi.org/10.1007/s13201-015-0367-y
33. Ling CM, Mohamed AR, Bhatia S (2004) Performance of photocatalytic reactors using immobilized TiO_2 film for the degradation of phenol and methylene blue dye present in water stream. Chemosphere 57:547–554. https://doi.org/10.1016/j.chemosphere.2004.07.011
34. Lai Z, Peng F, Wang H et al. (2013) A new insight into regulating high energy facets of rutile TiO_2. J Mater Chem A 1–4. https://doi.org/10.1039/c3ta00188a
35. Meng X, Shin D, Yu SM et al. (2014) Formation mechanism of Rutile TiO_2 rods on fluorine doped tin oxide. J Nanosci Nanotechnol 14:8839–8844. https://doi.org/10.1166/jnn.2014.10016
36. Huyen T, Chi T, Dung N et al. (2018) Enhanced photocatalytic activity of {110}-faceted TiO_2 rutile nanorods in the photodegradation of hazardous pharmaceuticals. Nanomaterials 8:276. https://doi.org/10.3390/nano8050276
37. Yusoff MM, Mamat MH, Ismail AS et al. (2018) Enhancing the performance of self-powered ultraviolet photosensor using rapid aqueous chemical-grown aluminum-doped titanium oxide nanorod arrays as electron transport layer. Thin Solid Films 655:1–12. https://doi.org/10.1016/j.tsf.2018.03.091
38. Mathews NR, Morales ER, Cortés-Jacome MA, Toledo Antonio JA (2009) TiO_2 thin films – Influence of annealing temperature on structural, optical and photocatalytic properties. Sol Energy 83:1499–1508. https://doi.org/10.1016/j.solener.2009.04.008
39. Santara B, Giri PK, Imakita K, Fujii M (2014) Microscopic origin of lattice contraction and expansion in undoped Rutile TiO_2 nanostructures. J Phys D Appl Phys 47:215302
40. Ahmad MK, Mokhtar SM, Soon CF et al. (2016) Raman investigation of rutile-phased TiO_2 nanorods/nanoflowers with various reaction times using one step hydrothermal method. J Mater Sci Mater Electron 27:7920–7926. https://doi.org/10.1007/s10854-016-4783-z
41. Hernandes J.V, Coste S, García A (2017) Effects of metal doping (Cu, Ag, Eu) on the electronic and optical behavior of nanostructured TiO_2 Journal of Alloys and Compound 710:355–363. https://doi.org/10.1016/j.jallcom.2017.03.275
42. Khan MM, Ansari SA, Pradhan D et al. (2014) Band gap engineered TiO_2 nanoparticles for visible light induced photoelectrochemical and photocatalytic studies. J Mater Chem 2:637–644. https://doi.org/10.1039/c3ta14052k
43. Zuo F, Bozhilov K, Dillon RJ et al. (2012) Active facets on titanium (III)-doped TiO_2: an effective strategy to improve the visible-light photocatalytic activity. Angew Chemie Int Ed 51:6223–6226. https://doi.org/10.1002/anie.201202191
44. Park H, Park Y, Kim W, Choi W (2013) Surface modification of TiO_2 photocatalyst for environmental applications. J Photochem Photobiol C Photochem Rev 15:1–20. https://doi.org/10.1016/j.jphotochemrev.2012.10.001
45. Daviosdóttir S, Dirscherl K, Canulescu S et al. (2013) Nanoscale surface potential imaging of the photocatalytic TiO_2 films on aluminum. RSC Adv 3:23296–23302. https://doi.org/10.1039/c3ra43082k
46. Lai YK, Sun L, Chen C et al. (2005) Optical and electrical characterization of TiO_2 nanotube arrays on titanium substrate. 252:1101–1106. https://doi.org/10.1016/j.apsusc.2005.02.035

47. Mathew S, Prasad AK, Benoy T et al. (2012) UV-visible photoluminescence of TiO2 nanoparticles prepared by hydrothermal method. J Fluoresc 22:1563–1569. https://doi.org/10.1007/s10895-012-1096-3
48. Xiong L, Li J, Yang B, Yu Y (2012) Ti3+ in the surface of titanium dioxide: generation, properties and photocatalytic application. J Nanomater. https://doi.org/10.1155/2012/831524
49. Pan X, Yang M, Zhang N (2013) Defective TiO_2 with oxygen vacancies: Synthesis, properties and photocatalytic applications. Nanoscale 5:3601–3614. https://doi.org/10.1039/c3nr00476g
50. Rajabi M, Shogh S, Iraji Zad A (2015) Defect study of TiO_2 nanorods grown by a hydrothermal method through photoluminescence spectroscopy. J Lumin 157:235–242. https://doi.org/10.1016/j.jlumin.2014.08.035
51. Pauly TR, Liu Y, Pinnavaia TJ et al. (1999) Textural mesoporosity and the catalytic activity of mesoporous molecular sieves with wormhole framework structures. J Am Chem Soc 121:8835–8842
52. Nakata K, Fujishima A (2012) TiO_2 photocatalysis: design and applications. J Photochem Photobiol C Photochem Rev 13:169–189. https://doi.org/10.1016/j.jphotochemrev.2012.06.001
53. Harish S, Archana J, Navaneethan M et al. (2016) Enhanced visible light induced photocatalytic activity on the degradation of organic pollutants by SnO nanoparticle decorated hierarchical ZnO nanostructures. RSC Adv 6:89721–89731. https://doi.org/10.1039/c6ra19824d
54. Cavigli L, Bogani F, Vinattieri A et al. (2009) Volume versus surface-mediated recombination in anatase TiO_2 nanoparticles. J Appl Phys 106:053516. https://doi.org/10.1063/1.3211291
55. Mustapha F, Jalil AA, Mohamed M et al. (2017) New insight into self-modified surfaces with defect-rich rutile TiO_2 as a visible-light-driven photocatalyst new insight into self-modified surfaces with defect-rich rutile TiO_2 as a visible-light-driven photocatalyst. J Clean Prod 168:1150–1162. https://doi.org/10.1016/j.jclepro.2017.09.095
56. Sabarinathan M, Harish S, Archana J et al. (2016) Controlled exfoliation of monodispersed MoS2 layered nanostructures by a ligand-assisted hydrothermal approach for the realization of ultrafast degradation of an organic pollutant. RSC Adv 6:109495–109505. https://doi.org/10.1039/c6ra24355j
57. Franco Arias LM, Arias Duran A, Cardona D, Camps E, Gómez GZ ME (2015) Effect of annealing treatment on the photocatalytic activity of TiO_2 thin films deposited by dc reactive magnetron sputtering. J Phys 614:1–6. https://doi.org/10.1088/1742-6596/614/1/012008
58. Dulian P, Nachit W, Jaglarz J et al. (2019) Photocatalytic methylene blue degradation on multilayer transparent TiO_2 coatings. Opt Mater (Amst) 90:264–272. https://doi.org/10.1016/j.optmat.2019.02.041
59. Retamoso C, Escalona N, González M et al. (2019) Effect of particle size on the photocatalytic activity of modified rutile sand (TiO_2) for the discoloration of methylene blue in water. J Photochem Photobiol A Chem 378:136–141. https://doi.org/10.1016/j.jphotochem.2019.04.021
60. Sun Y, Qian J, Zhao QR et al. (2021) Hydrothermal synthesis of rutile TiO_2 nanotubes film on Ti foil for photocatalytic degradation. Dig J Nanomater Biostructures 16:579–584
61. Hamed NKA, Ahmad MK, Mazlan MH et al. (2019) Low temperature fabrication of flower-like rutile phased TiO_2 film towards methyl orange degradation. Int J Eng Technol 8:49–55
62. Ahmad MK, Fitrah A, Aziz A et al. (2017) Rutile phased titanium dioxide (TiO_2) nanorod/nano flower based waste water treatment device. https://doi.org/10.1007/978-3-319-46490-9